Liquid Crystals
Publication details, including instructions for authors and subscription information:
http://www.informaworld.com/smpp/title~content=t713926090

Measurement of the pyroelectric response and of the thermal diffusivity of microtomized sections of 'single crystalline' ferroelectric liquid crystalline elastomers

Norbert Leister; Walter Lehmann; Uwe Weber; Dieter Geschke; Friedrich Kremer; Peter Stein; Heino Finkelmann

Online publication date: 06 August 2010

To cite this Article Leister, Norbert , Lehmann, Walter , Weber, Uwe , Geschke, Dieter , Kremer, Friedrich , Stein, Peter and Finkelmann, Heino(2000) 'Measurement of the pyroelectric response and of the thermal diffusivity of microtomized sections of 'single crystalline' ferroelectric liquid crystalline elastomers', Liquid Crystals, 27: 2, 289 — 297
To link to this Article: DOI: 10.1080/026782900203119
URL: http://dx.doi.org/10.1080/026782900203119

LIQUID CRYSTALS, 2000, VOL. 27, NO. 2, 289–297

Measurement of the pyroelectric response and of the thermal diffusivity of microtomized sections of 'single crystalline' ferroelectric liquid crystalline elastomers

NORBERT LEISTER*, WALTER LEHMANN, UWE WEBER, DIETER GESCHKE, FRIEDRICH KREMER

Universität Leipzig, Fakultät für Physik und Geowissenschaften, Institut für Experimentelle Physik I, Linnéstr. 5, 04103 Leipzig, Germany

PETER STEIN and HEINO FINKELMANN

Albrecht-Ludwigs-Universität Freiburg, Institut für Makromolekulare Chemie, Sonnenstr. 5, 79104 Freiburg, Germany

(*Received 27 July 1999; in final form 25 September 1999; accepted 16 October 1999*)

The pyroelectric response and the thermal properties of microtomized sections of 'single-crystalline' ferroelectric liquid crystalline elastomers (FLCE) have been investigated. The microtomized sections were manufactured in the thickness range from 20 to 100 µm. The roughness of the surfaces due to the cutting process was investigated with an alpha-stepper and found to be in the range of about 5 µm. The thermal diffusivity of the elastomer at different temperatures was determined by placing the sample on a pyroelectric substrate and measuring the pyroelectric signal of the substrate under appropriate conditions. From the pyroelectric current spectra, information about the spatial distribution of the polarization could be deduced. It was found to be constant except in a range also about 5 µm near the surface. From the combination of this result and that of the alpha-stepper measurements, the conclusion is drawn that the molecular orientation at the surface is destroyed due to the cutting process. The magnitude of the spontaneous polarization was calculated from the pyroelectric measurements at different temperatures, making use of the thermal diffusivity values.

1. Introduction

In ferroelectric liquid crystals, a spontaneous polarization exists in each smectic layer, but usually no macroscopic polarization can be observed in the bulk state due to a helical superstructure of the polarization vector from layer to layer. Surface stabilized states are limited to very thin samples. On the other hand in SmC* elastomers (see also [1–3]), the helical superstructure can be unwound and a macroscopically uniform alignment can be obtained by applying mechanical fields consistent with the symmetry of the SmC* phase [4–6]. Elastomer samples can be produced in sheets of several hundred micrometers thickness. Thinner samples can be obtained by microtome cutting of the original sheets. The investigations presented here deal with the determination of the macroscopic spontaneous polarization $\mathbf{P}_s$ of such microtome cut elastomer sheets.

*Author for correspondence; e-mail: leister@physik.uni-leipzig.de

2. Experimental

2.1. *Sample*

The single crystalline ferroelectric LC elastomer is a coelastomer with two different chiral mesogenic sub-units (see figure 1 for molecular structures) attached, comb-like, to a polysiloxane backbone. During the crosslinking of the siloxane backbones, the polymeric LC sample is subjected to two successive uniaxial deformations. The first deformation orients the mesogenic units and the second one, performed at a special angle (90°-θ) with respect to the first one, where θ is the tilt angle of the SmC* phase, orients the smectic layers uniformly [4–6]. This leads to a bookshelf geometry of the LC with a polar axis normal to the sample sheet. Microtome cutting was performed parallel to the plane of the sheet. Therefore, the sections have the same geometry as the original sheet.

2.2. *Experimental methods*

Two experimental methods are commonly used to determine the spontaneous polarization of a FLC material:

Liquid Crystals ISSN 0267-8292 print/ISSN 1366-5855 online © 2000 Taylor & Francis Ltd
http://www.tandf.co.uk/journals/tf/02678292.html

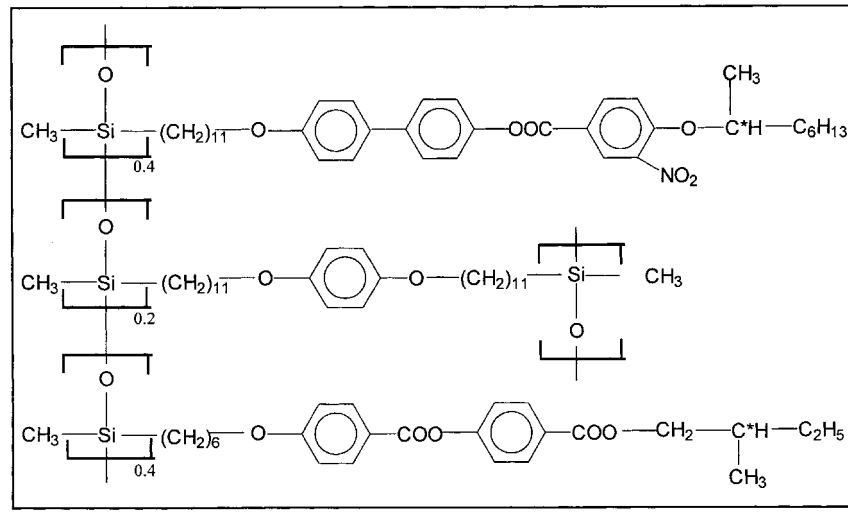

Figure 1. Molecular structure of the system under investigation. The LC elastomer has two different mesogenic subunits attached, comblike, to a polysiloxane backbone.

the triangular wave method [7] and pyroelectric investigations using the method introduced by Chynoweth [8]. In the triangular wave method, the polarization reversal current is detected when the sample is switched between the two ferroelectric states of opposite polarization. In pyroelectric measurements, the change of the polarization with temperature due to an induced time dependent heating of the sample is analysed.

Pyroelectric data are known to give a good representation of the *relative* temperature dependence of the spontaneous polarization. On the other hand it is also known that it is difficult to obtain *absolute* values of $\mathbf{P}_s$ from these measurements, because in general the magnitude of the temperature change ΔT inside the sample, caused by heating, is unknown (see for example [9–11]). Therefore, both methods are often combined: triangular wave measurements are made at only a few temperatures and the results are used to calibrate the $\mathbf{P}_s(T)$ data obtained from the pyroelectric measurements.

For crosslinked elastomer samples however, the use of the triangular wave method is often inapplicable because elastomers with a high crosslinking density are not switchable, and even in elastomers with low crosslinking densities, the long switching times do not allow determination of $\mathbf{P}_s$ from these measurements [12]. The polarization has to be determined from pyroelectric data alone.

Some authors [13] propose the following procedure to calibrate their data. Pyroelectric measurements are performed on a different material for which the absolute value of the polarization is known. The relative magnitude of the pyroelectric current values for the material under investigation and the reference material are compared. However, it has to be noted that the temperature change in a material due to a given amount of heat is proportional to the density and to the specific heat capacity of this material. Therefore a direct comparison of the pyroelectric current data for different materials may lead to errors.

The laser intensity modulation method (LIMM), developed by Lang and Das-Gupta [14, 15] is a derivative of the method of Chynoweth. LIMM was developed mainly in order to obtain spatially resolved information about the origin of the pyrosignal inside the sample. On the other hand, if the thermal properties of the material are known, absolute values of the polarization can be calculated from the LIMM data.

In the present paper, thermal diffusivity and LIMM measurements on microtome cut elastomer samples in the thickness range from 20 to 100 µm are combined. In this way, one can elucidate whether the mechanical orientation of the LC is homogeneous or varies with the depth into the sample. Furthermore, for the first time absolute values of the spontaneous polarization and its temperature dependence for this material can be given.

2.2.1. *Pyroelectric measurements*

The principle of the LIMM measurements [14, 16, 17] is as follows. The sample is placed between non-transparent metal electrodes that are vacuum deposited on a 2.5 µm thick Mylar foil. One electrode is irradiated by an intensity-modulated laser beam. The light absorption at the electrode leads to a corresponding modulated heat generation. The penetration depth of the resulting heat wave depends on the modulation frequency f. For small frequencies, the whole sample is heated almost homogeneously, and for high frequencies, the range of the heat modulation is concentrated near the irradiated surface. A temperature-induced change of the polarization inside the sample induces charges on the electrodes. Phase sensitive detection (lock-in amplifier) of the resulting

pyrocurrent is performed for different modulation frequencies. At each frequency, only the dipoles in the penetration range of the heat wave (approx. $\sim f^{-1/2}$) contribute to the current signal. Information about the spatial origin of the pyrosignal can then be obtained by numerical deconvolution of the current spectrum by use of the regularization method given in [16].

The pyroelectric current I_p at a fixed modulation frequency $f = \omega/2\pi$ can be written as

$$I_p(\omega) = i\omega \frac{A}{L} \int_0^L r(x)\Delta T(\omega, x)\,dx, \qquad r(x) = g(x) + bE(x) \tag{1}$$

where A is the electrode area, L the sample thickness, x the sample depth coordinate and $\Delta T(\omega, x)$ is the temperature profile. $r(x)$ has contributions from the pyroelectric coefficient $g(x) = d\mathbf{P}_s/dT$ and from the internal electric field $E(x)$ caused by possible charge concentrations in the sample (b is a material parameter dependent on thermal expansion and dielectric properties). However, if no external electric fields are applied, the mean value r_m does not include charge contributions and thus is equal to the mean pyroelectric coefficient g_m.

The temperature profile $\Delta T(\omega, x)$ in equation (1) is given by [16]:

$$\Delta T(\omega, x) = \frac{q_\sim \eta_a}{K\kappa} \frac{\cosh[K(L-x)] + a_L \sinh[K(L-x)]}{(a_0 + a_L)\cosh(KL) + (1 + a_0 a_L)\sinh(KL)}$$

$$a_{0,L} = \frac{H_{0,L}}{K\kappa}, \qquad K = (1+i)\left(\frac{\omega}{2\chi}\right)^{1/2}, \qquad \chi = \frac{\kappa}{\rho c_p} \tag{2}$$

where $q_\sim$ is the laser power density, η_a the absorption coefficient of the metal electrode, κ is the thermal conductivity of the sample, χ the thermal diffusivity, ρ the density and c_p is the specific heat capacity. H_0, H_L are the heat transfer coefficients at the front and rear side of the sample, respectively.

The experimental set-up used here has already been described in detail [16, 18]. The sample geometry is shown in figure 2.

The pyroelectric spectra (I_p as function of the modulation frequency) of the elastomer samples are recorded at 22°C (room temperature) and in the temperature range from 30 to 85°C in steps of 5 K (accuracy ± 0.3 K).

2.2.2. *Thermal diffusivity measurements*

According to equation (2), $\Delta T(\omega, x)$ depends on two thermal quantities of the material investigated, the thermal conductivity κ and the thermal diffusivity χ. In principle, both quantities can be determined from the pyroelectric current spectrum and from the profile $r(x)$ which is obtained from the regularization method [19, 20]. In an iterative procedure, the residual between the measured current spectrum and the spectrum recalculated from the $r(x)$ profile is minimized. However, in most cases this data evaluation process is not very precise.

In the investigations presented here, one of the two thermal quantities, the thermal diffusivity χ of the elastomer, has been determined in an independent measurement leaving only the thermal conductivity κ to be calculated. The method described by Ploss *et al.* is used [21]. In order to obtain a value for the diffusivity, the temperature modulation at both sample surfaces $\Delta T(\omega, x = 0)$ and $\Delta T(\omega, x = L)$ has to be measured for different modulation frequencies. By calculation of $\Delta T(\omega, x = 0)$ and $\Delta T(\omega, x = L)$ according to equation (2), one obtains the fraction a of both temperature spectra

$$a = \frac{\Delta T(\omega, x = 0)}{\Delta T(\omega, x = L)} = \cosh(KL) + \frac{H_L}{K\kappa}\sinh(KL),$$

$$K = (1+i)\left(\frac{\omega}{2\chi}\right)^{1/2}. \tag{3}$$

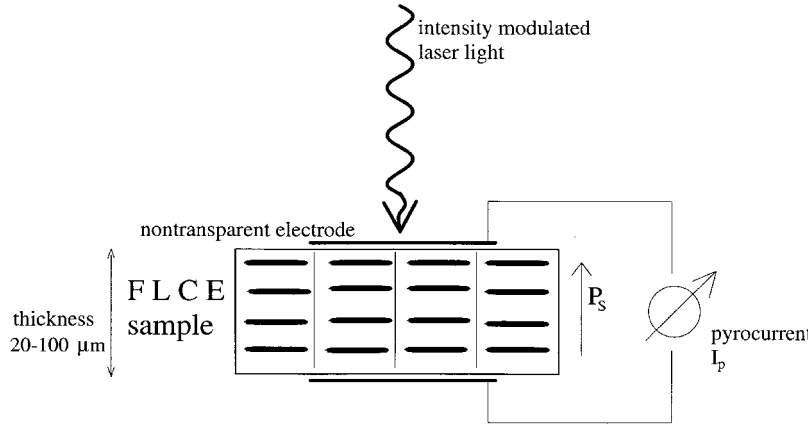

Figure 2. Experimental geometry for the pyroelectric measurements. The single crystalline ferroelectric LC elastomers (thickness 20–100 µm for different samples) have a bookshelf geometry. The mesogenic units are tilted in the plane of the sample sheet. The vector of the spontaneous polarization points in the thickness direction.

For large frequencies $f = \omega/2\pi \gg \chi/\pi L^2$ the approximation $\cosh(KL) \approx 1/2 \exp(KL)$ can be made. Furthermore $H_L/\kappa K \ll 1$ holds for large K. This leads to the following equations for the absolute value $|a|$ and the phase $\phi(a)$ of the complex fraction a in equation (3)

$$\ln|a| \approx \frac{\pi^{1/2} L}{\chi^{1/2}} f^{1/2} - \ln 2, \qquad \phi(a) = \frac{\pi^{1/2} L}{\chi^{1/2}} f^{1/2}. \quad (4)$$

Both expressions are dependent only on the measurement frequency, the sample thickness and the thermal diffusivity. If $\ln|a|$ and $\phi(a)$ are plotted against the square root of the modulation frequency (as shown in figure 4 for example) the thermal diffusivity can be obtained from a linear fit in the frequency range where both curves are parallel.

Bauer and Ploss [21, 22] have proposed different experimental set-ups for the measurement of χ. In a first one [22] ΔT is determined by measuring the temperature-induced changes of the resistivity of the metal electrodes. However, our results obtained with this method show that the signals are small which leads to a poor signal to noise ratio.

In the second set-up [21], the material under investigation is placed onto a PVDF-foil (polyvinylidene fluoride), which is used as pyroelectric substrate (see figure 3). Pyroelectric current spectra are recorded with the same experimental set-up as in the usual LIMM measurements. The PVDF-foil has been electrically poled by the manufacturer (Solvay) resulting in a high pyroelectric response. It is equipped with electrodes in the usual way (see [17]). The elastomer sample is placed onto the upper electrode. In the first part of the measurement, an additional metal layer (consisting of gold and indium) is placed on the upper surface of the elastomer sheet, figure 3(*a*). The pyroelectric current between the PVDF electrodes, caused by laser light absorption in this upper metal layer, is measured. The pyrosignal arises from the heat which has passed through the elastomer sheet and penetrated into the PVDF-foil. This is equivalent to measuring the temperature $\Delta T(\omega, x = L)$ on the rear surface of the elastomer. Then the metal layer on the elastomer surface is carefully removed and a second measurement made, where the laser light transmits through the elastomer and is absorbed on the upper electrode of the PVDF foil. This is equivalent to measuring the temperature $\Delta T(\omega, x = 0)$ on the front surface of the elastomer.

The applicability of this method is limited to materials which are transparent. Besides, a good thermal contact between the material under investigation and the PVDF foil is necessary. Both conditions are fulfilled for the elastomer. The use of PVDF with its large pyrosignal gives a sufficient signal to noise ratio. The data are recorded in the frequency range 10–300 Hz and for the same temperatures as the pyroelectric current spectra.

3. Results and discussion

3.1. *Diffusivity measurements*

Figure 4 shows the data $\ln|a|$ and $\phi(a)$ according to equation (4) calculated from the complex fraction a of the two current measurements, at room temperature and plotted against the square root of the modulation frequency. At small frequencies one can see the expected deviation from linearity, as the approximation $f \gg \chi/\pi L^2$ for equation (4) is not valid in this frequency range. At high frequencies there is also a deviation from linearity, especially for the $\phi(a)$ values, which cannot be explained from the theory. However, the temperature modulation at the rear side $\Delta T(\omega, x = L)$, proportional to the denominator of the fraction a, is, according to equation (2),

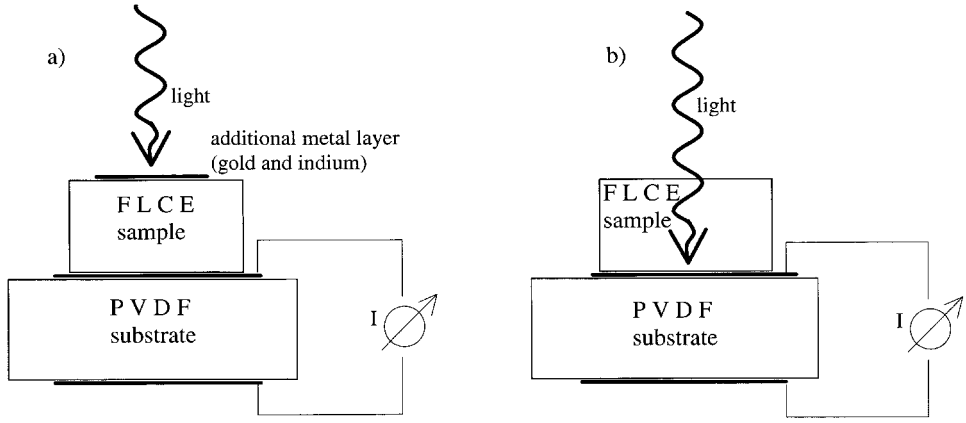

Figure 3. Set-up for the thermal diffusivity measurements according to Ploss *et al.* [21]. The elastomer sheet is placed onto a PVDF foil, which acts as pyroelectric substrate. The pyroelectric current signals of the substrate are measured (*a*) for light absorption on an additional metal layer on top of the elastomer sheet and (*b*) for light absorption on the electrode for the PVDF foil.

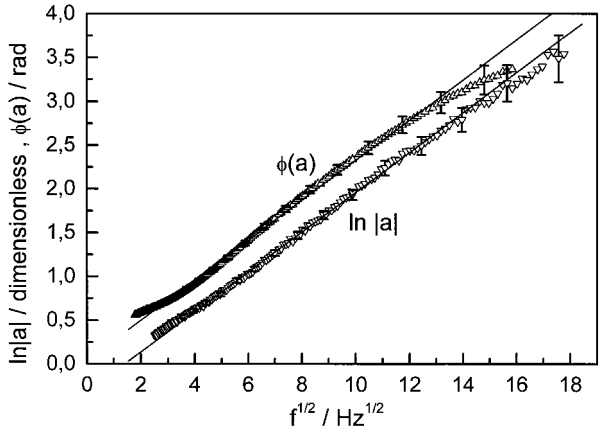

Figure 4. $\ln|a|$ and $\phi(a)$ values calculated from the (complex) ratio a of the two current measurements described in figure 3, at room temperature. The data are plotted against the square root of the modulation frequency. Also shown are the linear fits for both curves. From the fit value the thermal diffusivity χ can be calculated according to equation (4).

very small at higher frequencies. Therefore, with rising frequency the result becomes more sensitive to errors.

Nevertheless both curves show a linear shape at intermediate frequencies and linear fits can be made leading to almost identical results. A fit $y = m^* f^{1/2} + b$ results in $m = 0.228$ for the $\ln|a|$ curve and $m = 0.229$ for the $\phi(a)$ curve. A value for χ can then be calculated from m using the relation $\chi = \pi L^2/m^2$ according to equation (4). In this case $\chi = 3.7 \times 10^{-8}$ m^2 s^{-1} results. Corresponding fits have been performed for the data from the measurements at other temperatures. The resulting temperature dependence of χ is plotted in figure 5: χ shows a slight decrease up to temperatures of about 55°C and is almost constant at higher temperatures. The values of about $2.4–3.7 \times 10^{-8}$ m^2 s^{-1} are in the order of magnitude usually found for polymer foils. For example for the PVDF foil $\chi = 6.2 \times 10^{-8}$ m^2 s^{-1} was determined, which is in accordance with [21].

3.2. *Thickness variation of the samples*

The error in the determination of χ is given by the quality of the fits according to equation (4), but also depends on errors in the determination of the sample thickness L. Besides the absolute value of L, a variation of the sample thickness over the investigated area may contribute to the error. Of course such a thickness variation would also lead to errors in the determination of the profile $r(x)$ from the pyroelectric data. The sample sheets used were obtained by microtome cutting. The quality of the sheets may be influenced by the cutting process. Therefore the samples were checked for thickness variations with an alpha-stepper. They were put on a glass plate serving as a solid and smooth background and cross-sections of the sample thickness were determined.

Figure 6 shows a measured cross-section. The sample thickness varies in the range between about 21 μm and 25 μm over the observed distance of approximately 1.5 mm. From the data at different positions, a mean value 22.6 ± 1.4 μm can be calculated. These results show that a thickness variation is present, but is limited to a tolerable amount.

Because the thermal diffusivity depends quadratically on the thickness, the relative thickness variation $\Delta L/L$ of 6% for this sample results in a contribution to the relative error of the diffusivity $\Delta\chi/\chi$ of 12%.

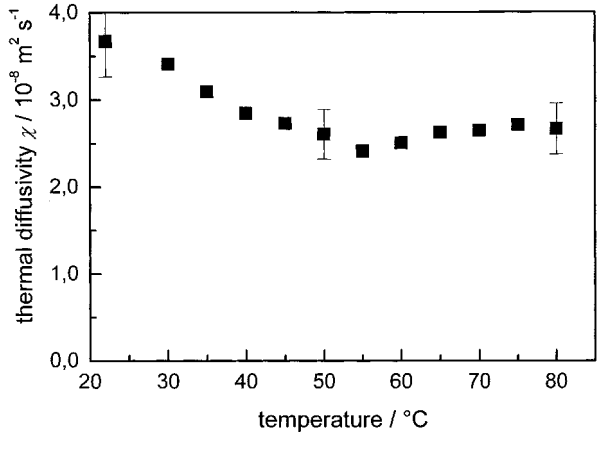

Figure 5. Values for the thermal diffusivity χ after the method of Ploss (figure 3) at different temperatures. The first point on the left side has been calculated from the fit data in figure 4.

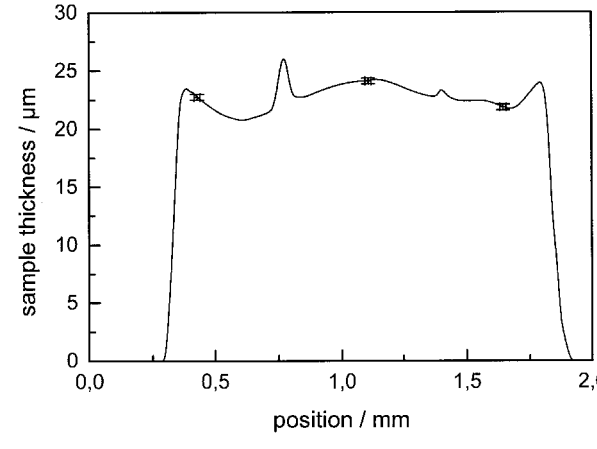

Figure 6. Cross-section of the sample thickness of an elastomer sheet over the area investigated. The roughness is in a range of about 5 μm; the average thickness is 22.6 μm. (Alpha-stepper data: DEKTAK 3030, stylus tip radius: 12 μm.)

3.3. *Pyroelectric measurements*

3.3.1. *The profile r(x)*

Figure 7 shows a measured pyroelectric current spectrum and the profile $r(x)$ calculated from these measurements using the regularization method given in [16]. In this case the sample consists of a 39 µm thick elastomer sheet between two 2.5 µm mylar foils. The real part of the spectrum shows a maximum at low frequencies (20 Hz) and drops down in the range from 100 Hz to 1 kHz. As the measurement frequency is correlated to the penetration depth of the thermal waves, one can derive from the data that the surface region of the sample contributes to the signal to a small amount. The penetration depth of 2.5 µm at the border between mylar foil and elastomer corresponds to a frequency of about 4 kHz.

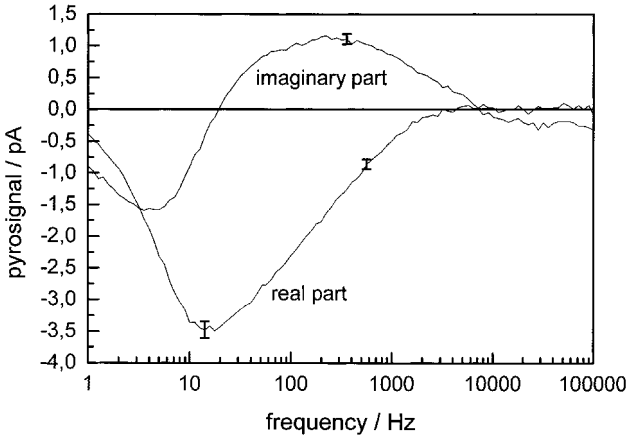

(*a*)

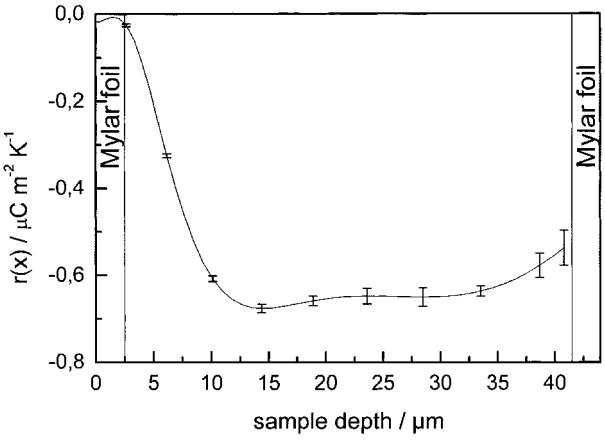

(*b*)

Figure 7. (*a*) Real and imaginary parts of a pyroelectric current spectrum at room temperature. (*b*) Depth profile $r(x)$ calculated from the spectrum in (*a*) by the regularization method [16], making use of the value for the thermal diffussivity χ at room temperature (first point on the left side in figure 5). $r(x)$ gives information about the spatial origin of the pyrosignal. As the pyrosignal arises from the spontaneous polarization, a location in the sample showing lower values for $r(x)$ is attributed to having lower polarization. Except for the rough (5 µm) surface, the polarization and therefore the orientation of the LC is almost homogeneous inside the sample. Total sample thickness: 44 µm (39 µm elastomer sheet and two 2.5 µm mylar foils. Interface mylar/elastomer is indicated by vertical lines).

The profile $r(x)$ was calculated from these data, using the result for χ given above. It is characterized by an almost constant $r(x)$ value inside the sample and a decrease on the left side in a range of about 10 µm from the outer surface or 7.5 µm from the surface of the elastomer layer; $r(x)$ is approximately zero inside the mylar foil. The signal decreases again at the rear side of the sample (right side in the figure). The fact that it does not fall to zero there is due to numerical effects and the decreasing resolution of the method far away from the irradiated surface. As discussed in detail in [17], by calculating the profiles $r(x)$ numerical smoothing and broadening are inevitable. On the other hand, the region on the left side which shows lower values of $r(x)$ is very broad and the measured spectrum gives clear evidence that the surface region exhibits less pyroelectric response than the inner parts of the sample. These results are supported by the fact that 10 µm thick elastomer samples showed no pyroelectric response at all.

Having observed a roughness of about 5 µm in the alpha-stepper measurements and a range with small pyroelectric response near the surface, one can conclude that the microtome cutting process does destroy the molecular orientation near the surface.

3.3.2. *The temperature dependence of the pyroelectric response*

Measurements at different temperatures did not show a significant change in the shape of the measured current spectra, as can be seen in figure 8. On the other hand, the magnitude of the signal changes due to the temperature dependence of the pyroelectric coefficient. A rise in the signal can be found up to about 55°C. For higher temperatures, the signal decreases again, but a non-zero signal remains up to 85°C.

The phase sequence of the corresponding non-crosslinked polymer is g-13 SmX* 43 SmC* 59 SmA* 75 I (°). Usually the pyrosignal vanishes at the phase transition SmC* to SmA* for measurements performed under short circuit conditions, as is done here [18].

The phase sequence given above was determined from microscopic texture investigations for the uncrosslinked sample. For the crosslinked materials, a determination of phase transitions from optical investigations is not possible. DSC data for the elastomer do not show a significant change of the glass transition temperature (− 13°C)

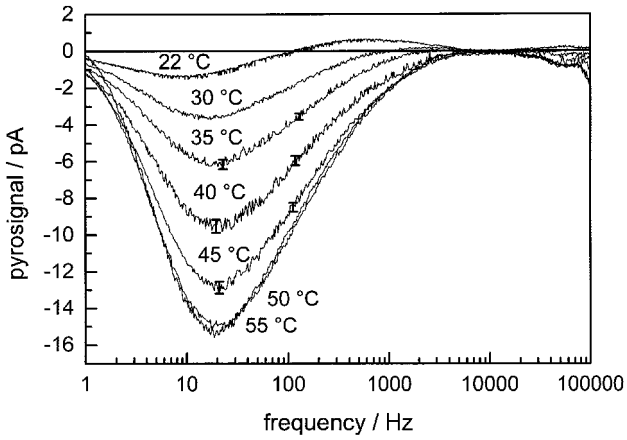

(*a*)

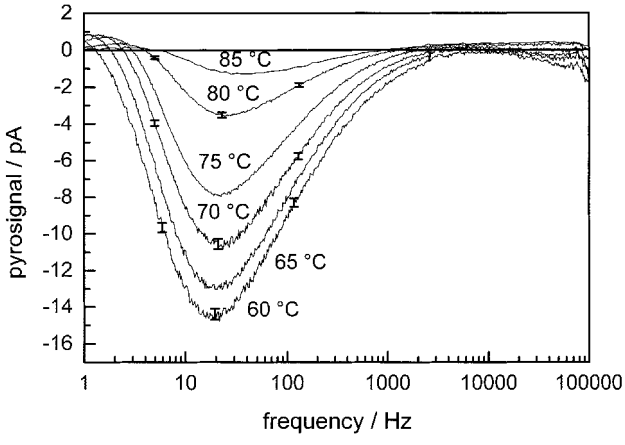

(*b*)

Figure 8. Temperature dependence of the pyroelectric signal (*a*) 22–55°C (SmX* and SmC* phase of the uncrosslinked FLC polymer); (*b*) 60–85°C (SmA* and isotropic phase of the uncrosslinked FLC polymer). Even at temperatures that correspond to the SmA* phase for the uncrosslinked FLC polymer, a polarization is observed in the FLC elastomer; this is assigned to a residual tilt angle due to crosslinking.

and the transition temperature SmX* → SmC* due to crosslinking. The second order transition SmC* → SmA* cannot be investigated by DSC; this phase transition can be broadened due to crosslinking. Due to the network structure part of the orientation remains at higher temperatures.

X-ray data (figure 9) and second harmonic generation data [23] indicate different structures in the temperature ranges below and above 60°C. Figure 9 shows the X-ray diffraction pattern (small angle region) of the elastomer after the first uniaxial deformation. At this stage of the orientation process the smectic layers are oriented at an

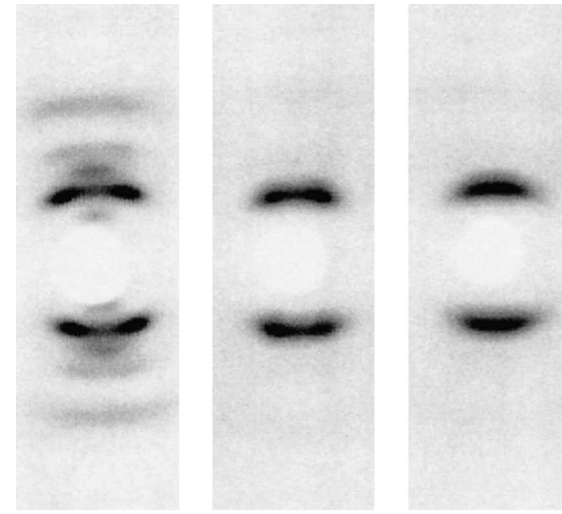

Figure 9. Small angle region of the X-ray pictures of the elastomer after the first uniaxial deformation. At this stage of the orientation process the smectic layers are oriented at an angle $\pm\Theta$ with respect to the stress direction, but due to the conical layer distribution the elastomer has no macroscopic C-2 symmetry. (*a*) at 25°C, (*b*) at 55°C, (*c*) at 65°C. The data shown in (*a*) and (*b*) show tilted structures; (*c*) indicates an *average* tilt of 0°.

angle $\pm\Theta$ with respect to the stress direction, but due to the two possible layer orientations, the elastomer has no macroscopic C-2 symmetry [6]. Figure 9 (*a*) taken at 25°C (SmX* phase) and figure 9 (*b*) taken at 55°C (SmC* phase) show two maxima on the left and on the right side. The angle between these maxima corresponds to twice the tilt angle. The X-ray diffraction pattern at 65°C, figure 9 (*c*), indicates an *average* tilt of zero, but the reflections are broad and small residual tilt angles are not resolved. From these data it is rather probable that SmC* contributions are still present above 60°C.

The non-vanishing pyroelectric response at temperatures that correspond to the SmA* phase of the uncrosslinked polymer is consistent with the temperature dependence of the piezoelectric response [24]. Therefore the pyroelectric and piezoelectric results are of prime importance to the conclusion that the phase transition is actually broadened. There exists a residual tilt angle in the SmA* phase due to the so-called 'mechanoclinic effect' of the elastic network [12, 25].

A value of the spontaneous polarization of this new material can be obtained by integrating the pyrocoefficients calculated for different temperatures with the Curie temperature T_c as upper integration limit.

$$P(T) = \int_{T}^{T_c} g(T')\,\mathrm{d}'T. \qquad (5)$$

In this case, the integration has been performed up to the temperature at which the pyrosignal vanishes. For each temperature, the profile $r(x)$ has been calculated from the pyroelectric spectrum (making use of the corresponding χ value for this particular temperature) and the mean values $r_m = g_m$ have been integrated. The result obtained from the measured data in figure 8 is shown in figure 10. A value of about 12 nC cm^{-2} at room temperature results. This value is about one order of magnitude smaller than for some polymeric liquid crystals with very high polarization [26]; on the other hand, it is larger than the values found for some different elastomers [13]. (The orientation of the elastomer after the second uniaxial deformation can also be checked by X-ray measurements [6, 23, 24]. In fact, there is a distribution of the layer orientations with a maximum in the ideal, i.e. bookshelf, position [24].)

In an error estimation, in addition to the error values for L and χ, the relative errors for the thermal conductivity κ of 15%, and the relative error of the absorptivity η_a of the metal electrode of 13% have to be taken into account, leading to relative errors of 24% for the g_m values. For the determination of the polarization, the relative accuracy of the temperature steps of 6% has to be considered in addition, leading to a relative error of 25% for $\mathbf{P}_s$.

Measurements have been performed for five samples of different thicknesses. The values for the spontaneous polarization at room temperature vary between 6.5 nC cm^{-2} (55 μm sample) and 16 nC cm^{-2} (100 μm sample). This range of $\mathbf{P}_s$ is broader than expected from the statistical error of the measurement or from the somewhat greater influence of microtome cutting effects in thinner samples, and can be attributed to differences in the degree of orientation of the LC in different sections of the elastomer samples. The data obtained lead to an average value of the spontaneous polarization of 11.2 ± 4.2 nC cm^{-2}.

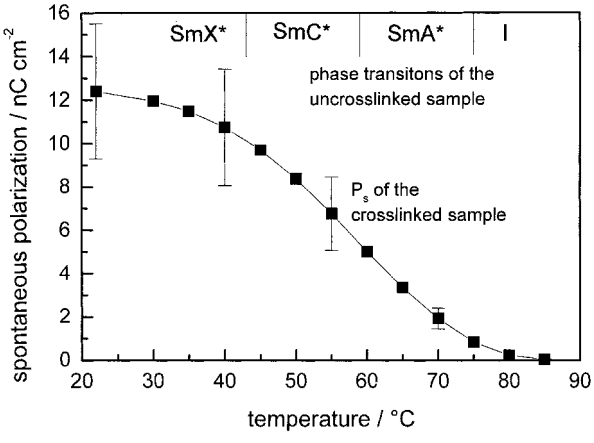

Figure 10. Temperature dependence of the spontaneous polarization, calculated from the data in figure 8. From the pyroelectric data it is concluded that the phase transitions of the material broaden during crosslinking. There exists a residual tilt angle in the SmA* phase due to the 'mechanoclinic effect' of the network (elastic memory) [12, 25].

4. Conclusions

Microtome cut elastomer sheets in the thickness range 20–100 μm have been investigated. Alpha-stepper measurements have shown, that the thickness variation over the area of the sheets is limited to a range of about 5 μm. With pyroelectric investigations and the help of additional thermal diffusivity measurements, it was possible for the first time to calculate the magnitude of the spontaneous polarization in these samples with a relative accuracy of 25%. As the applicability of the triangular wave method to crosslinked elastomers is limited to switchable elastomers with low crosslinking density, pyroelectric investigations are of major importance in the determination of the polarization for these materials. The determination of thermal material parameters enables us to give an absolute value of $\mathbf{P}_s$ from pyroelectric data alone.

The average value for the polarization found here is 11.2 ± 4.2 nC cm^{-2}. For the first time, the thermal diffusivity of the material has been determined to be $\chi = 3.7 \pm 0.4\ 10^{-8}$ m^2 s^{-1} at room temperature.

Support by the DFG-project Ge 718/4-2 and the Innovationskolleg 'Phänomene an den Miniaturisierungsgrenzen' is gratefully acknowledged. G. Ramm is gratefully acknowledged for performing the alpha-stepper measurements.

References

[1] Skupin, H., Kremer, F., Shilov, S., Stein, P., and Finkelmann, H., 1991, *Macromolecules*, **32,** 3746.
[2] Brodowsky, H. M., Boehnke, U.-C., Kremer, F., Gebhardt, E., and Zentel, R., 1997, *Langmuir*, **13,** 5378.
[3] Brodowsky, H. M., Boehnke, U.-C., Kremer, F., Gebhardt, E., and Zentel, R., 1999, *Langmuir*, **15,** 274.
[4] Semmler, K., and Finkelmann, H., 1994, *Polym. Adv. Technol.*, **5,** 231.
[5] Semmler, K., and Finkelmann, H., 1995, *Macromol. Chem. Phys.*, **196,** 3197.
[6] Eckert, T., Finkelmann, H., Keck, M., Lehmann, W., and Kremer, F., 1996, *Macromol. Chem. rapid Commun.*, **17,** 767.
[7] Miyasato, K., Abe, S., Takezoe, H., Fukuda, A., and Kuze, E., 1983, *Jpn. J. appl. Phys.*, **22,** L661.
[8] Chynoweth, A. G., 1956, *J. appl. Phys.*, **27,** 78.
[9] Glass, A. M., Patel, J. S., Goodby, J. W., Olson, D. H., and Geary, J. W., 1986, *J. appl. Phys.*, **60,** 2778.
[10] Skarp, K., Andersson, G., Zentel, R., and Poths, H., 1995, *Proc. SPIE*, **2408,** 32.
[11] Dierking, I., Andersson, G., Komitov, L., Lagerwall, S. T., and Stebler, B., 1997, *Ferroelectrics*, **193,** 1.

[12] Brehmer, M., Zentel, R., Gießelmann, F., Germer, R., and Zugenmaier, P., 1996, *Liq. Cryst.*, **21,** 589.
[13] Mauzac, M., Nguyen, H. T., Tournilhac, F. G., and Yablonsky, S. V., 1995, *Chem. Phys. Lett.*, **240,** 461.
[14] Lang, S. B., and Das-Gupta, D. K., 1986, *J. appl. Phys.*, **59,** 2151.
[15] Lang, S. B., 1991, *Ferroelectrics*, **118,** 343.
[16] Bloß, P., and Schäfer, H., 1994, *Rev. sci. Instrum.*, **65,** 1541.
[17] Leister, N., and Geschke, D., 1998, *Liq. Cryst.*, **24,** 441.
[18] Leister, N., Geschke, D., and Kozlovsky, M. V., 1998, *Mol. Cryst. liq. Cryst.*, **309,** 201.
[19] Steffen, M., Bloß, P., and Schäfer, H., 1994, in Proceedings of the 8th International Symposium on Electrets, ISE8, edited by J. Lewiner, D. Morisseau, and C. Alquié, p. 200.
[20] Bloß, P., Steffen, M., Schäfer, H., Eberle, G., and Eisenmenger, W., 1996, *IEEE Transactions on Dielectrics and Electrical Instruments*, **3,** 417.
[21] Ploss, B., Bauer, S., and Bon, C., 1991, *Ferroelectrics*, **118,** 435.
[22] Bauer, S., and Ploss, B., 1990, *J. appl. Phys.*, **68,** 6361.
[23] Bennè, I., Semmler, K., and Finkelmann, H., 1995, *Macromolecules*, **28,** 1854.
[24] Lehmann, W., Hartmann, L., Kremer, F., Stein, P., Finkelmann, H., Kruth, H., and Diele, S., 1999, *J. appl. Phys.*, **86,** 1647.
[25] Stein, P., 1999, PhD thesis, Universität Freiburg, Germany.
[26] Dubois, J. C., Le Barny, P., Mauzac, M., and Noel, C., 1997, *Acta Polym.*, **48,** 47.